ACS Chemical Neuroscience

Research Article

pubs.acs.org/chemneuro

Phosphorylation of α3 Glycine Receptors Induces a Conformational Change in the Glycine-Binding Site

Lu Han,[†] Sahil Talwar,[†] Qian Wang,[†] Qiang Shan,[†,§] and Joseph W. Lynch*[,†,‡]

[†]Queensland Brain Institute and [‡]School of Biomedical Sciences, The University of Queensland, Brisbane QLD 4072, Australia

Supporting Information

ABSTRACT: Inflammatory pain sensitization is initiated by prostaglandin-induced phosphorylation of α3 glycine receptors (GlyRs) that are specifically located in inhibitory synapses on spinal pain sensory neurons. Phosphorylation reduces the magnitude of glycinergic synaptic currents, thereby disinhibiting nociceptive neurons. Although α1 and α3 subunits are both expressed on spinal nociceptive neurons, α3 is a more promising therapeutic target as its sparse expression elsewhere implies a reduced risk of side-effects. Here we compared glycine-mediated conformational changes in α1 and α3 GlyRs to identify structural differences that might be exploited in designing α3-specific analgesics. Using voltage-clamp fluorometry, we show that glycine-mediated conformational changes in the extracellular M2-M3 domain were significantly different between the two GlyR isoforms. Using a chimeric approach, we found that structural variations in the intracellular M3-M4 domain were responsible for this difference. This prompted us to test the hypothesis that phosphorylation of S346 in α3 GlyR might also induce extracellular conformation changes. We show using both voltage-clamp fluorometry and pharmacology that Ser346 phosphorylation elicits structural changes in the α3 glycine-binding site. These results provide the first direct evidence for phosphorylation-mediated extracellular conformational changes in pentameric ligand-gated ion channels, and thus suggest new loci for investigating how phosphorylation modulates structure and function in this receptor family. More importantly, by demonstrating that phosphorylation alters α3 GlyR glycine-binding site structure, they raise the possibility of developing analgesics that selectively target inflammation-modulated GlyRs.

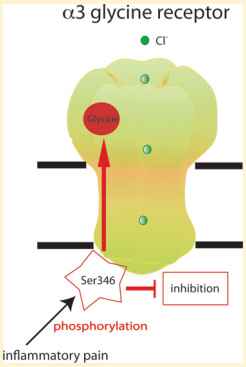

KEYWORDS: *pLGIC, Cys-loop receptor, inflammatory pain, glycinergic synapse, electrophysiology, protein conformation*

Members of the pentameric ligand-gated ion channel (pLGIC) receptor family mediate fast synaptic transmission in the nervous system. The cation-permeable nicotinic acetylcholine receptor (nAChR) is the most intensively studied member of this family, with other members including the anion-permeable glycine and GABA type-A receptors (GlyRs and $GABA_A$Rs) and the cation-permeable serotonin type-3 receptor ($5\text{-}HT_3R$).[1] Functional pLGICs comprise an assembly of five homologous membrane-spanning subunits arranged symmetrically around a central pore. All subunits incorporate large N-terminal ligand-binding domains that form neurotransmitter-binding sites at the interface of adjacent domains. The eponymous extracellular Cys-loop is conserved among eukaryotic members of this family. In addition, GlyRs incorporate a second Cys-loop that forms the C loop ligand-binding domain that is crucial for glycine binding.[2] The ligand-binding domain is followed by four transmembrane α-helices, termed M1−M4, that each span the entire thickness of the cell membrane. Each subunit contributes an M2 domain to the lining of the axial water-filled pore. To facilitate comparison of pore-lining residues between different pLGIC members, a common M2 residue numbering system is used which assigns 1′ and 19′ to the innermost and outermost pore-lining residues, respectively. The M1, M2, and M3 domains are connected by short loops. The intracellular domain linking M3 and M4 varies considerably in both length and amino acid sequence among different pLGIC subunits.

Although GlyRs are best known for mediating inhibitory neurotransmission in reflex circuits of the spinal cord, they also mediate inhibitory neurotransmission onto spinal nociceptive neurons in superficial laminae of the spinal cord dorsal horn. GlyR α3 subunits, which are otherwise sparsely distributed, are abundantly expressed in these synapses.[3] Chronic inflammatory pain sensitization is caused in part by a prostaglandin E_2 (PGE_2)-mediated activation of protein kinase A (PKA), which in turn phosphorylates α3 GlyRs at S346, leading to a diminution of glycinergic synaptic current magnitude.[3,4] This disinhibits spinal nociceptive sensory neurons resulting in chronic inflammatory pain sensitization. Due to their sparse distribution outside the spinal cord dorsal horn, α3 GlyRs have emerged as preferred therapeutic targets for chronic pain,[5,6] and agents that potentiate α3 GlyRs have been shown to exhibit analgesic efficacy in animal models of chronic inflammatory pain.[7]

Our original aim was to compare glycine-induced conformational changes in α1 and α3 GlyRs in an attempt to identify structural differences that could be exploited in the design of α3-specific potentiators. To achieve this, we employed voltage-clamp fluorometry (VCF) to quantitate conformational changes occurring in the immediate vicinity of residues labeled

Received: April 29, 2013
Accepted: July 8, 2013
Published: July 8, 2013

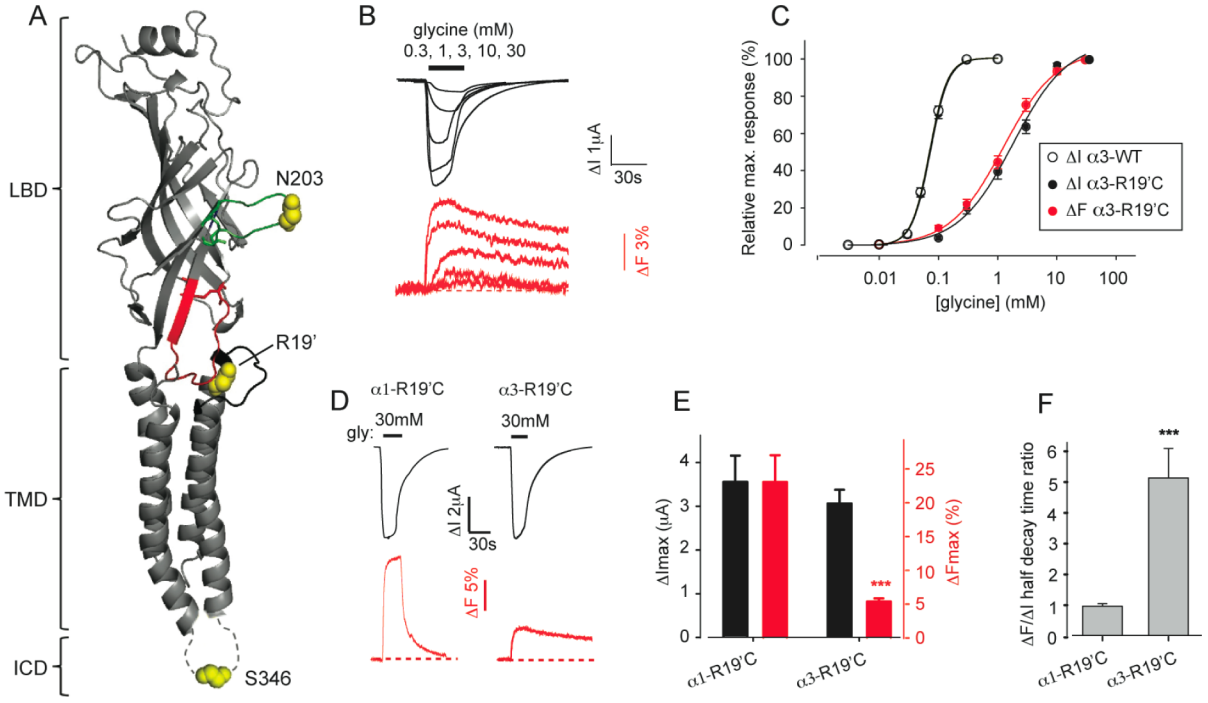

Figure 1. Comparison of fluorescence properties of MTSR-labeled α1-R19′C and α3-R19′C GlyRs. In this and all subsequent figures, ΔI and ΔF recordings are shown in black and red, respectively. (A) Structural model of an α3 GlyR subunit showing R19′, S346, and N203 as main chain atoms in yellow. Other structures indicated include the loop C glycine-binding domain (green), the conserved Cys-loop (red), and the M2-M3 domain (black). The location of S346 is indicative only as the M3-M4 domain which houses this residue is yet to be structurally determined and is displayed here as a dashed loop. The ligand-binding domain (LBD), transmembrane domain (TMD), and intracellular domain (ICD) are delineated as indicated. The model was generated as recently described[37] and rendered in Pymol. (B) Examples of glycine ΔI and ΔF dose−response relationships recorded from an oocyte that expressed MTSR-labeled α3-R19′C GlyRs. (C) Averaged ΔI and ΔF dose−response relations for the MTSR-labeled α3-R19′C GlyR together with the averaged ΔI dose−response relation for the MTSR-labeled α3-WT GlyR. Mean parameters of best fit to the dose−response curves are given in Table S1. (D) Sample recordings from α1-R19′C and α3-R19′C GlyRs showing typical differences in the magnitude and decay rates of ΔF_{max} responses. (E) Comparison of averaged ΔI_{max} and ΔF_{max} values. (G) Comparison of ΔF_{max} decay rates. In this analysis, the ΔF_{max} half-decay times were ratioed with the corresponding ΔI_{max} half-decay times to normalize for possible differences in ΔI decay rate between α1 and α3 GlyRs. ***$p < 0.001$ compared to the α1-R19′C GlyR by unpaired t test.

with environmentally sensitive fluorophores. Initially, we probed glycine-induced conformational changes at a fluorescent reporter attached at the external end (R271 or R19′) of the M2 pore-lining domain. This revealed differences in glycine-induced conformations in α1 and α3 GlyRs that, to our surprise, were due to structural variations in their M3-M4 domains. This prompted us to investigate whether PKA-induced phosphorylation of S346 (in the α3 GlyR M3-M4 domain) may also produce extracellular conformational changes. Phosphorylation of S346 was found to induce conformational changes not only at the external end of M2, but also in the glycine-binding site.

RESULTS AND DISCUSSION

We employed VCF to compare glycine-induced conformational changes in α1 and α3 receptors in an attempt to identify structural differences that could be exploited in the design of α3-specific potentiators as analgesics. For these studies, we employed the GlyR human α1 and rat α3L subunit cDNAs (Figure S1, Supporting Information) with UniProt accession numbers of P23415-2 (i.e., isoform b) and P24524, respectively. Both constructs incorporated the C41A mutation that eliminated the sole uncross-linked extracellular sulfhydryl group. The C41A mutation has no effect on receptor function.[8,9] Constructs incorporating only this mutation are termed wild type (WT). We initially compared the glycine-induced fluorescence responses of a methanethiosulfonate-rhodamine (MTSR) reporter covalently attached to R19′C in the α1 and α3 GlyRs. Although the R19′C mutation impairs the glycine gating efficacy of the α1 GlyR,[8−10] we employed it here for two reasons: First, R19′ forms part of the M2-M3 loop which is known to be intimately involved in receptor gating.[11,12] Hence, if α1 and α3 GlyRs exhibit distinct quaternary structures, this difference should be reflected in their gating mechanisms and hence R19′C should be a promising location for detecting these. Second, R19′C is the only known gating site that when fluorescently labeled gives a glycine-induced fluorescence change (ΔF) large enough to be quantitatively analyzed.[9] The maximum glycine-induced fluorescence response (ΔF_{max}) in the MTSR-labeled α1-R19′C GlyR is about 20%.[9] By comparison, application of a saturating (30 mM) glycine concentration to MTSR-labeled α3-R19′C GlyRs elicited a ΔF_{max} of 5.1 ± 1.0% (n = 13). As no detectable ΔF was ever observed in wild type (WT) MTSR-labeled α1-WT or α3-WT GlyRs (Table S1, Supporting Information), we conclude that the α3-R19′C GlyR is specifically labeled by MTSR.

A structural model of an α3 GlyR subunit displaying the location of R19′ and the M2-M3 loop is presented in Figure 1A. As previously observed for the α1-R19′C GlyR,[9] glycine current (ΔI) and ΔF dose−response relationships were almost overlapping in α3-R19′C GlyRs (Figure 1B, C). Indeed, using a

dx.doi.org/10.1021/cn400097j | ACS Chem. Neurosci. 2013, 4, 1361−1370

paired t test, the mean glycine ΔI half-maximal concentration (EC_{50}) of 1740 ± 270 μM (n = 13) was not significantly different from the mean glycine ΔF EC_{50} of 1340 ± 210 μM (n = 13). However, both values were significantly larger than the corresponding α3-WT GlyR ΔI glycine EC_{50} value (74 ± 2 μM, n = 6) using an unpaired t test (P < 0.001 for both). Sample recordings of ΔF_{max} responses from MTSR-labeled α3-R19′C GlyRs suggested that they were smaller in magnitude and slower to decay to baseline than those recorded from MTSR-labeled α1-R19′C GlyRs (Figure 1D). Averaged results confirmed that ΔF_{max} responses from α3-R19′C GlyRs were significantly reduced in magnitude, although their saturating current magnitude (ΔI_{max}) values were not significantly different (P > 0.08 by unpaired t test) (Figure 1E). We quantified ΔF decay rates by determining the ratio of the ΔF_{max} half-decay time to the ΔI_{max} half-decay time in the same oocyte to control for possible differences in ΔI_{max} decay rate between receptor subtypes. As shown in Figure 1F, ΔF_{max} did indeed decay at a significantly slower rate in MTSR-labeled α3-R19′C GlyRs relative to MTSR-labeled α1-R19′C GlyRs. These differences were surprising because the amino acid sequences of α1 and α3 subunits are identical in all domains that are likely to come into contact with a rhodamine attached at the 19′C position.

Due to this unexpected finding, we compared the effects of a variety of pharmacological modulators on ΔF_{max} responses of MTSR-labeled α1-R19′C and α3-R19′C GlyRs. Although taurine and β-alanine are both very low efficacy agonists of α3-R19′C GlyRs, they elicit disproportionately large ΔF increases.[9] Consistent with this, although saturating taurine evoked no ΔI in α3-R19′C GlyRs (Figure S2A), it evoked mean ΔF_{max} near 25% of that produced by a saturating glycine concentration (Figure S2B, Table S1). Similarly, saturating β-alanine evoked a very small ΔI_{max} but a large ΔF_{max} that was ∼50% of that produced by saturating glycine (Figure S2A and B, Table S1). To facilitate comparison with glycine-mediated responses, Figure S2B shows mean ΔI and ΔF concentration−response relationships for glycine, β-alanine, and taurine with all averaged ΔI_{max}, ΔF_{max}, EC_{50}, and Hill coefficient (n_H) values summarized in Table S1. All variables corresponded closely to those recorded from MTSR-labeled α1-R19′C GlyRs under similar experimental conditions.[9]

Ivermectin, which irreversibly activates α1 and α3 GlyRs,[13,14] was previously shown to activate MTSR-labeled α1-R19′C GlyRs without inducing a detectable ΔF.[9] Here we found that saturating (15 μM) ivermectin evoked slowly activating currents in MTSR-labeled α3-R19′C GlyRs although detectable ΔF was observed (Figure S2C).

Finally, we compared the effects of the allosteric inhibitor, picrotoxin, and the classical competitive antagonist, strychnine. When applied alone, picrotoxin did not evoke significant ΔI or ΔF changes in oocytes expressing MTSR labeled α3-R19′C GlyRs (Figure S2D). However, when coapplied with EC_{50} glycine, 50 μM picrotoxin potently inhibited the current, although the ΔF increased significantly (17.3 ± 2.7%, n = 6). Strychnine also had no effect when applied alone, but significantly reduced ΔF by 48.7 ± 7.6% (n = 6) when coapplied with EC_{50} glycine (Figure S2E). The effects of both drugs on the direction of ΔF responses are consistent with those observed at MTSR-labeled α1-R19′C GlyRs.[9] From all these results, we infer that rhodamine labels attached to α1-R19′C and α3-R19′C GlyRs respond similarly to a variety of pharmacological manipulations, with the main difference being that α3-R19′C GlyRs exhibit smaller glycine-induced ΔF_{max} values and slower ΔF decay rates.

To isolate the domain responsible for the differential ΔF response characteristics, we initially generated a series of six chimeras, labeled Chi1−Chi6 as shown in Figure 2A. Each chimera was constructed from three variable modules: a ligand-binding domain, an M1-M3 transmembrane bundle plus large intracellular M3-M4 domain, and an M4 plus short C-terminal tail. A cysteine was introduced at the R19′C position of each chimera. The cDNAs for all chimeras were subcloned into the pGEMHE oocyte expression vector and functionally expressed in oocytes. Glycine ΔI and ΔF dose−response relationships were measured for all six chimeras, and all mean glycine EC_{50}, n_H, ΔI_{max}, and ΔF_{max} values are summarized in Table S2. Mean ΔI_{max} values were similar for all six chimeras (Figure 2B). However, the $\Delta F/\Delta I$ half-decay time ratios and ΔF_{max} values of three chimeras (Chi3, Chi5, Chi6) were all similar to those of α1-R19′C GlyRs, whereas those of the other three chimeras (Chi1, Chi2, Chi4) were significantly different from α1-R19′C GlyRs but similar to those of α3-R19′C GlyRs (Figure 2C, D). These results indicate that the differences in ΔF response characteristics can be transposed from the α1 to the α3 GlyR (and vice versa) by transposing the M1-M3 transmembrane bundle plus M3-M4 domain.

The M1-M3 transmembrane bundle amino acid sequences are very highly conserved between α1 and α3 GlyRs, with nonconserved residues existing only at I240 and G254 of the α1 subunit (residue numbering is the same for both subunits). The corresponding residues in the α3 GlyR are valine and alanine. To determine whether either of these was responsible for the differential ΔF response, we investigated the α1-R19′C-I240 V, α1-R19′C-G254A, α3-R19′C-V240I, and α33-R19′C-A254G double mutant GlyRs. However, as these mutations produced no significant change in ΔF properties, we generated another two chimeras (ChiA and ChiB, Figure 2A) where only the M3-M4 domains were exchanged. The mean glycine EC_{50}, n_H, ΔI_{max}, and ΔF_{max} values for ChiA and ChiB receptors, measured both before and after MTSR-labeling, are summarized in Table S2. Mean ΔI_{max} and ΔF_{max} responses of both chimeras, plus those of the original α1-R19′C and α3-R19′C GlyRs, are shown in Figure 2B and C. The ΔI_{max} of labeled ChiA was significantly reduced relative to those of both α1-R19′C and α3-R19′C GlyRs, possibly implying impaired surface expression. Nevertheless, the results for ChiB unequivocally indicate that transposing the M3-M4 domain from the α1-R19′C into the α3-R19′C GlyR produces an increased ΔF_{max} similar to that of the α1-R19′C GlyR (Figure 2C, D). Similarly, analysis of the $\Delta F/\Delta I$ half-decay time ratios indicated that this value can also be transferred between receptors by transferring their M3-M4 domains (Figure 2D). Thus, these results indicate that the primary structure of the M3-M4 domain influences tertiary structure in the immediate vicinity of a rhodamine label attached to R19′C (Figure 1A).

We next hypothesized that dynamic changes in M3-M4 loop conformation may also influence receptor conformation near R19′C. A PKA phosphorylation site has been identified at S346 in the α3 GlyR M3-M4 domain.[3] To determine whether phosphorylation of this site alters the microenvironment of a rhodamine attached to α3-R19′C, we investigated the effects of two mutations to this residue: S346G to eliminate the PKA site and S346E to mimic phosphorylation. The mean glycine EC_{50}, n_H, ΔI_{max} and ΔF_{max} values for the unlabeled and MTSR-labeled α3-R19′C−S346E and α3-R19′C−S346G double

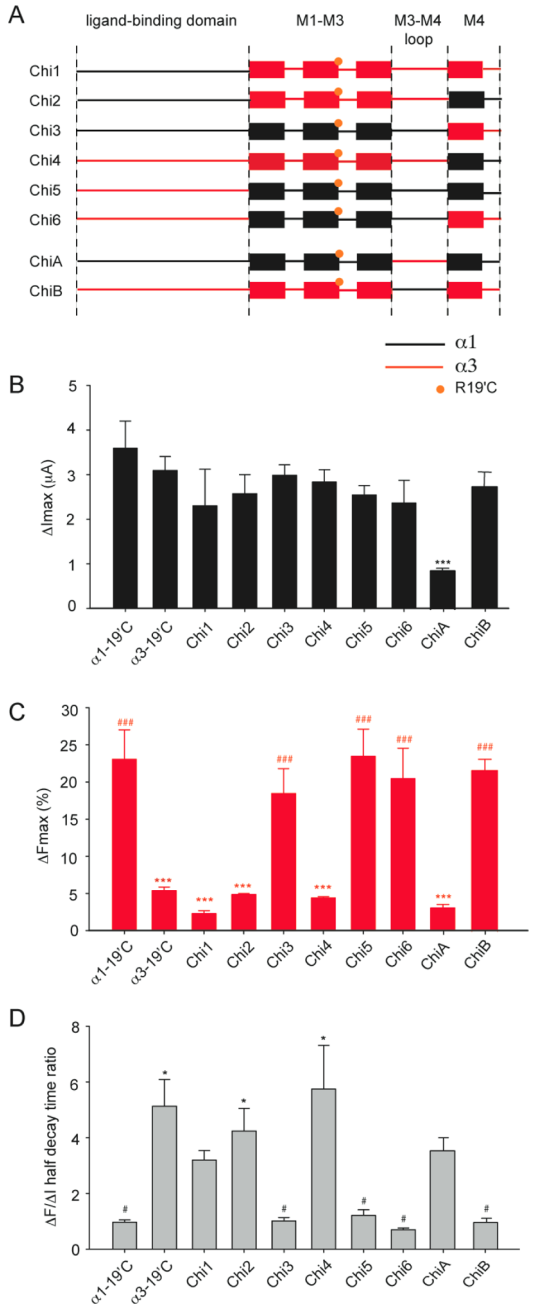

Figure 2. Comparison of ΔI and ΔF properties of eight chimeras composed of α1-R19′C and α3-R19′C GlyR domains. (A) Schematic illustration of the chimera structure. Domains from α1 and α3 GlyRs are colored black and red, respectively. Transmembrane α-helices are indicated by boxes with other regions shown as solid lines. The location of R19′C is indicated by an orange circle. The locations of the boundaries between the α1 and α3 sequences for each chimera are detailed above. Results shown in panels (B)−(D) are averaged from 5−12 oocytes. (B) Mean ΔI_{max} values of the indicated constructs. $^{***}p < 0.001$ compared to the α1-R19′C GlyR by unpaired t test (C) Mean ΔF_{max} values of the indicated constructs. $^{***}p < 0.001$ and $^{\#\#\#}p < 0.001$ compared to α1-R19′C GlyR and α3-R19′C GlyR, respectively, by one way ANOVA followed by Dunnett's post hoc test. (D) Mean $\Delta F_{max}/\Delta I_{max}$ half-decay time ratios of the indicated constructs. $^{*}p < 0.05$ and $^{\#}p < 0.05$ compared to α1-R19′C GlyR and α3-R19′C GlyR, respectively, by one way ANOVA followed by Dunnett's post hoc test.

mutant GlyRs are summarized in Table S2. The mean ΔI_{max} and ΔF_{max} values presented in Figure 3A indicate that ΔI_{max} was not significantly affected by either mutation, suggesting no effect on surface expression levels. However, the mean ΔF_{max} was significantly reduced in α3-R19′C−S346E GlyRs (Figure 3A). Moreover, the $\Delta F/\Delta I$ half-decay time ratio was significantly faster in the α3-R19′C−S346G GlyR than in the α3-R19′C or α3-R19′C−S346E GlyRs (Figure 3B). Thus, the phosphorylation-mimicking S346E mutation shifted both ΔF characteristics (i.e., peak magnitude and decay rate) from α1-like to α3-like, whereas eliminating the site (i.e., S346G) produced the reverse trend. From this result, we hypothesized that phosphorylation should reduce ΔF_{max} and possibly also prolong the ΔF half-decay time in MTSR-labeled α3-R19′C GlyRs.

We tested this directly by treating α3-R19′C GlyRs with 20 μM forskolin for 15 min to phosphorylate S346. As shown in the sample recording in Figure 3C, forskolin reversibly inhibited the ΔF induced by EC_{50} glycine in α3-R19′C GlyRs. A control experiment revealed that forskolin produced no significant change in ΔF magnitude in phosphorylation-deficient α3-R19′C-S346G GlyRs (Figure 3D), ruling out the possibility of nonspecific forskolin effects on ΔF. Similarly, application of 20 μM forskolin to α1-R19′C GlyRs produced percentage changes in ΔI_{max} and ΔF_{max} of 105 ± 8% and 95 ± 11% (both n = 20), neither of which was significant using a paired t test ($P > 0.1$ for both). A control dimethyl sulfoxide application to α3-R19′C GlyRs revealed that the incomplete recovery of the ΔF response following forskolin treatment was either a time- or solvent-dependent effect (Figure 3E, left), most likely representing fluorophore bleaching. As the EC_{50} glycine ΔI magnitude remained constant throughout each experiment (Figure 3C−E), we can rule out an effect of phosphorylation on GlyR surface expression levels or glycine sensitivity. Averaged results shown in Figure 3E (center and right panels) confirmed that forskolin inhibited the ΔF response of α3-R19′C GlyRs by ∼50%, but had no effect on α3-R19′C-S346G GlyRs. Together, these results indicate that phosphorylation of S346 induced a conformational change in the immediate vicinity of the rhodamine attached to R19′C in the α3 GlyR. The direction of this ΔF change is in accordance with that elicited by the phosphorylation-mimicking S346E mutation.

As phosphorylation induces a conformation change in or around the M2-M3 loop, we hypothesized that it may induce a global conformational change that propagates to the glycine-binding site. To test this, we investigated the effects of forskolin on glycine- and strychnine-induced ΔF responses in α3-N203C GlyRs that had been labeled by the sulfhydryl-reactive 2-((5(6)-tetramethylrhodamine)carboxylamino)ethyl methanethiosulfonate (MTS-TAMRA). There were three reasons for choosing this site. First, N203 lies at the "tip" of the loop C glycine-binding domain (Figure 1A) that is thought to close around the agonist as it binds in its subunit interface pocket.[15−17] Second, MTS-TAMRA-labeled α1-N203C GlyRs elicit large ΔFs (>40%) in response to the binding of either glycine or strychnine.[18] Third, unlike R19′C, the N203C mutation does not affect glycine sensitivity.[18] We first quantified the glycine ΔI and ΔF dose−response relationships in unlabeled and MTS-TAMRA-labeled α3-N203C and α3-N203C−S346G GlyRs, with all mean glycine EC_{50}, n_H, ΔI_{max} and ΔF_{max} values summarized in Table S3. Both mutants exhibited similar ΔI_{max} values which were not affected by MTS-

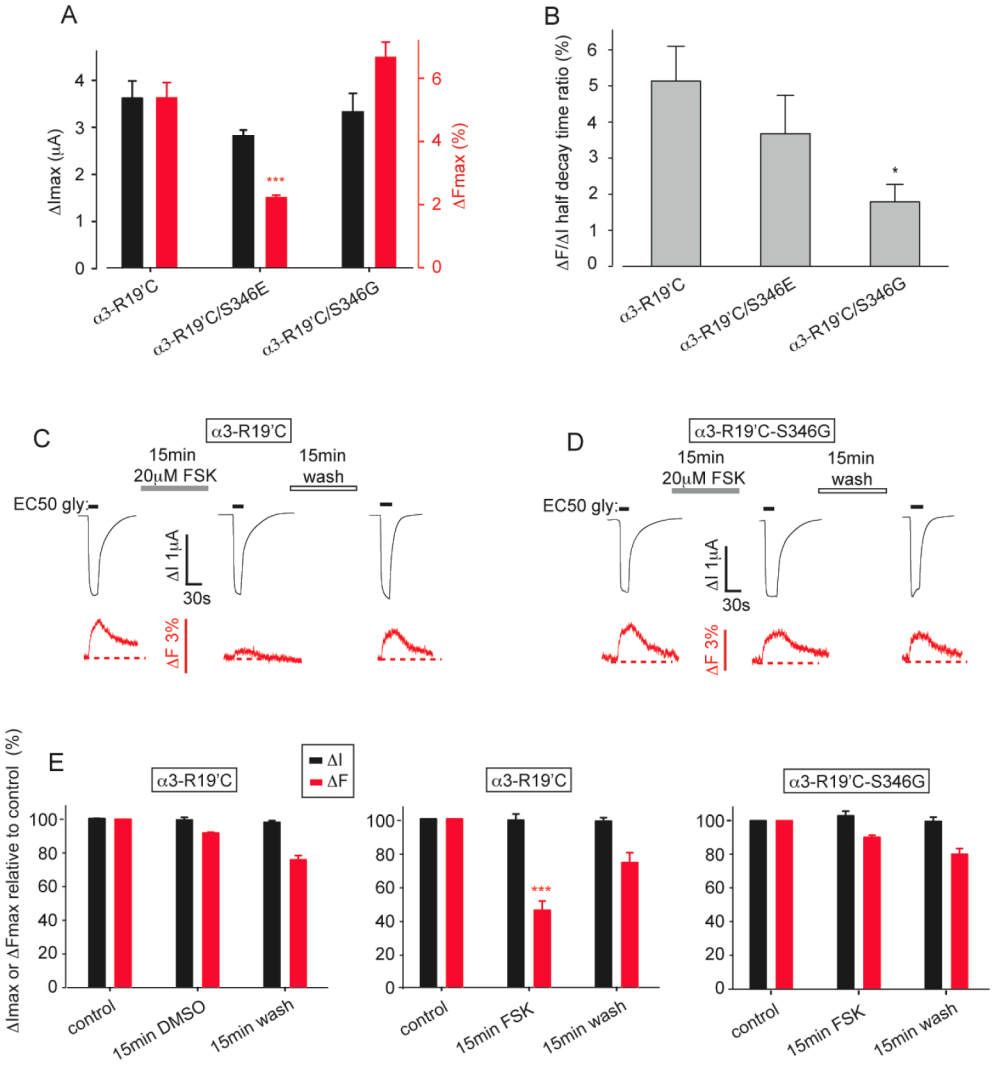

Figure 3. Effect of phosphorylation on ΔF responses of MTSR-labeled α3-R19′C GlyRs. (A) Comparison of ΔI_{max} and ΔF_{max} values in MTSR-labeled α3-R19′C, α3-R19′C-S346E and α3-R19′C-S346G GlyRs. ***$p < 0.001$ compared to α3-R19′C GlyR using unpaired t test. No significant differences were found for current magnitudes or for the increase in ΔF_{max} at the α3-R19′C-S346G GlyRs ($P > 0.10$). (B) Comparison of $\Delta F_{max}/\Delta I_{max}$ half-decay time ratios in the same three receptors. *$p < 0.05$ in α3-R19′C-S346G GlyR compared to α3-R19′C GlyR using unpaired t test. There was no significant difference between any other receptor pair ($P > 0.10$). (C) Examples of EC_{50} glycine-induced ΔI and ΔF responses in MTSR-labeled α3-R19′C GlyRs before and after a 15 min forskolin (FSK) treatment and after a 15 min wash. (D) Examples of EC_{50} glycine-induced ΔI and ΔF responses in MTSR-labeled α3-R19′C-S346G GlyRs before and after a 15 min forskolin treatment and after a 15 min wash. (E) Averaged data for the experiments shown in (C) and (D) (all $n = 5$). In addition, the effects of a control 15 min dimethyl sulfoxide (DMSO) treatment and wash on α3-R19′C GlyRs is also shown (left panel, all $n = 4$). *$p < 0.05$, ***$p < 0.001$ compared to control using paired t test.

TAMRA labeling. However, ΔF_{max} values were significantly larger in labeled α3-N203C-S346G GlyRs than in labeled α3-N203C GlyRs (7.1 ± 0.5 vs 4.0 ± 0.4%, $p < 0.05$ by unpaired t test, $n = 5$ oocytes each). The ΔF_{max} values induced by saturating (10 μM) strychnine were also significantly larger in α3-N203C-S346G GlyRs (8.4 ± 0.2 vs 5.4 ± 0.3%, $p < 0.001$ by unpaired t test, $n = 5$ oocytes each).

To determine whether phosphorylation induces a conformational change in the vicinity of a label attached to N203C, we tested the effects of a 15 min application of 20 μM forskolin on MTS-TAMRA-labeled α3-N203C and α3-N203C−S346G GlyRs. As shown in Figure 4A and B, forskolin reversibly reduced both glycine- and strychnine-mediated ΔF_{max} responses in labeled α3-N203C GlyRs. Nonspecific effects were eliminated on the grounds that forskolin had no significant effect on strychnine-mediated ΔF_{max} responses in α3-N203C-S346G GlyRs (Figure 4C). Forskolin did, however, have a small but statistically significant effect on glycine- mediated ΔF_{max} responses in α3-N203C−S346G GlyRs (Figure 4C, right). We thus infer that phosphorylation of S346 induces a conformational change in or near the α3 GlyR glycine-binding site.

We next investigated whether the rhodamine attached to N203C could detect molecular changes occurring within the glycine-binding pocket. For this, we employed two β-carboline derivatives, harmane and 6-methoxyharmalan, that differ in structure only by a methyoxy group at the C6 position (Figure S3A). These compounds, which are competitive antagonists of glycine, are predicted to bind in the glycine-binding site pocket in almost identical orientations.[19] Saturating (200 μM) concentrations of both β-carbolines elicited ΔF decreases in MTS-TAMRA-labeled α3-N203C GlyRs (Figure S3B), with the average ΔF_{max} induced by 6-methoxyharmalan being significantly larger than that induced by harmane (−3.7 ± 0.4 vs −1.0 ± 0.04%, $p < 0.05$ by unpaired t test, $n = 5$ oocytes

dx.doi.org/10.1021/cn400097j | ACS Chem. Neurosci. 2013, 4, 1361−1370

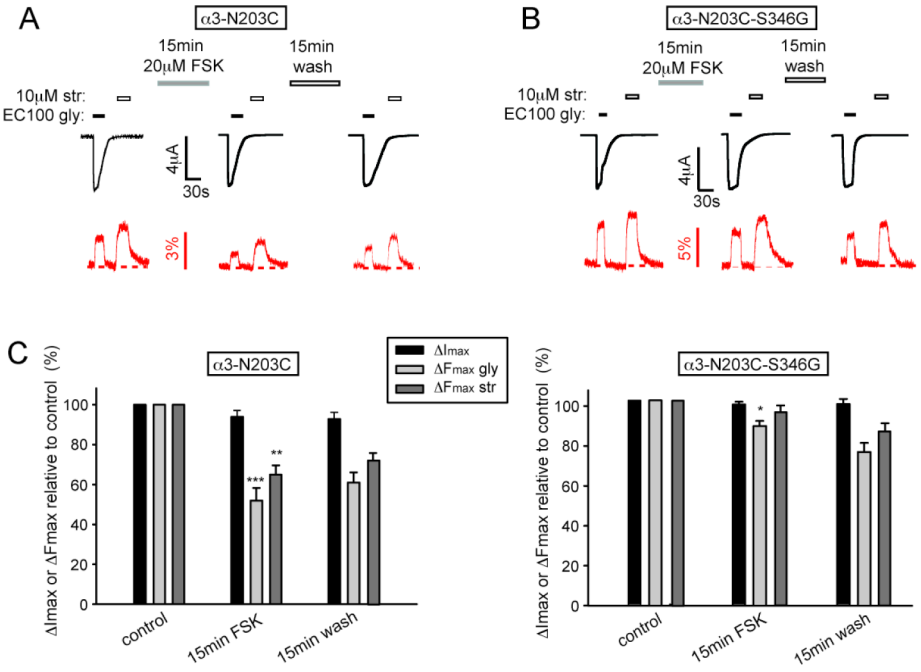

Figure 4. Effects of phosphorylation on ΔF responses induced by glycine and strychnine in MTS-TAMRA-labeled α3-N203C GlyRs. (A) Examples of glycine- and strychnine-induced ΔI_{max} and ΔF_{max} responses in MTS-TAMRA-labeled α3-N203C GlyRs before and after a 15 min forskolin treatment and after a 15 min wash. (B) Corresponding experiments on MTS-TAMRA-labeled α3-N203C−S346G GlyRs. (C) Averaged data for the experiments shown in A and B (all $n = 5$). *$p < 0.05$, **$p < 0.01$, ***$p < 0.001$ relative to control using paired t test.

each). Moreover, forskolin treatment inhibited the 6-methoxyharmalan-mediated ΔF_{max}, although it had no effect on that produced by harmane (Figure S3B,D). Differential responses were also observed in α3-N203C-S346G GlyRs, with 6-methyoxyharmalan and harmane eliciting ΔF_{max} values of −4.5 ± 0.5 and +0.6 ± 0.1%, respectively ($P < 0.05$ by unpaired t test, $n = 5$ oocytes each). As expected, forskolin elicited either insignificant, or small but significant, effects on the ΔF_{max} responses elicited by either compound in phosphorylation-deficient α3-N203C-S346G GlyRs (Figure S3C,D). These data indicate that a fluorophore attached to N203C successfully reports the addition of a small methoxy moiety into the glycine-binding pocket.

We then applied the same procedure to investigate the competitive antagonist, tropisetron, which is structurally unrelated to the β-carbolines (Figure S3A) but also binds in the glycine-binding pocket.[20,21] In the MTS-TAMRA-labeled α3-N203C and α3-N203C-S346G GlyRs, saturating (1 mM) tropisetron induced mean ΔF_{max} responses of +3.3 ± 0.3 and +7.3 ± 0.5%, respectively ($P < 0.05$ by unpaired t test, $n = 5$ oocytes each). As shown in Figure S3B−D, phosphorylation also reduced the tropisetron-induced ΔF_{max} response in α3-N203C GlyRs.

The above results are consistent with phosphorylation inducing a conformational change in or near the glycine-binding pocket. To determine whether it produces a conformational change inside the pocket, we quantified the effect of phosphorylation on the efficacy with which tropisetron, 6-methoxyharmalan, and harmane inhibited EC_{20} (40 μM) glycine-activated ΔI's in α3-WT GlyRs. This experiment also avoids the use of chemically modified receptors. As shown in Figure 5, the potency with which 150 μM tropisetron and 100 μM 6-methoxyharmalan inhibited α3-WT GlyRs was significantly and reversibly enhanced by phosphorylation. In contrast, the inhibition produced by 60 μM harmane was not affected by phosphorylation. Consistent with results from the α3-R19′C and α3-N203C GlyRs described above (Figures 3E, 4C), glycine-gated ΔI's in α3-WT GlyRs were not affected by phosphorylation. Thus, the results strongly suggest that phosphorylation induces a conformational change in the glycine-binding site.

Given that S346 phosphorylation inhibits α3-WT GlyRs expressed in mammalian HEK293 cells[3,7] but not in *Xenopus* oocytes, it is evident that this effect is expression system specific. It was therefore relevant to determine whether phosphorylation also induces a conformational change in the glycine-binding site of HEK293 cell-expressed α3-WT GlyRs. As it is not feasible to perform VCF experiments on HEK293 cells due to the high level of nonspecific fluorophore labeling, we employed a pharmacological approach only. Specifically, we continually monitored the inhibitory potency of a 20 μM (~IC_{50}) concentration of tropisetron on EC_{50} (180 μM) glycine-activated ΔI's before, during, and after forskolin treatment. Figure 6A shows a typical recording, together with expanded sections of the traces recorded before and immediately after forskolin exposure. It shows that forskolin simultaneously reduced ΔI magnitude and enhanced tropisetron potency. Results averaged from six cells confirm both effects and demonstrate their reversibility after a 15 min wash (Figure 6B, C). In contrast, when applied to α1-WT GlyRs, forskolin was never observed to elicit a detectable response (defined as a >10% change in current over a 10 min application period) in each of 10 cells in which it was examined. As tropisetron is a competitive antagonist, it is possible that its enhanced potency in could be due to a phosphorylation-mediated reduction in glycine affinity in HEK293 cells. We tested this directly by applying alternating EC_{50} (180 μM) and EC_{100} (1 mM) concentrations of glycine to α3-WT GlyRs before, during and after the period of forskolin exposure (Figure 6D). As forskolin inhibited EC_{100} currents to a

dx.doi.org/10.1021/cn400097j | ACS Chem. Neurosci. 2013, 4, 1361−1370

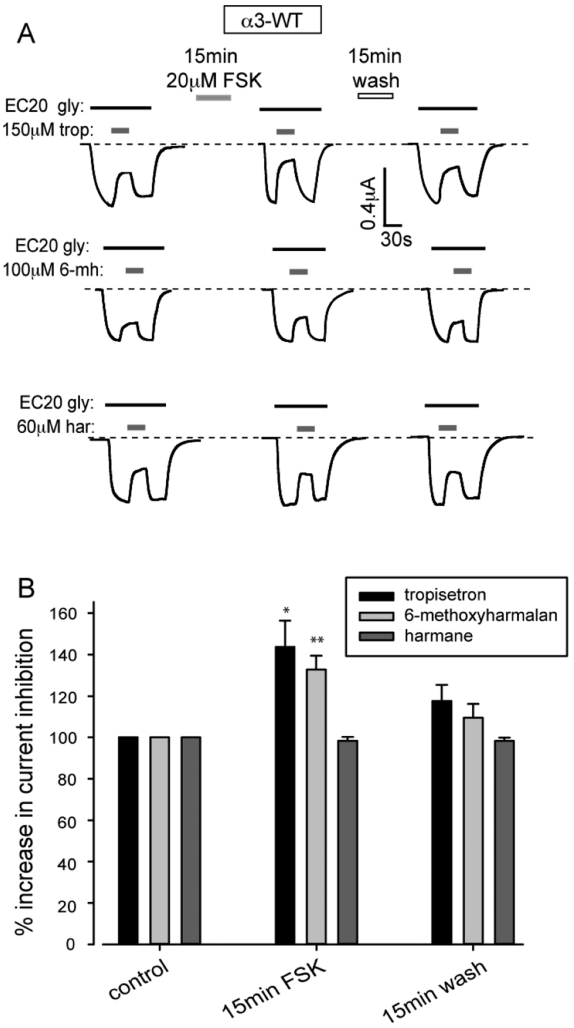

Figure 5. Effects of phosphorylation on the inhibitory potencies of tropisetron, 6-methoxyharmalan, and harmane in α3-WT GlyRs. (A) Examples of the inhibitory effects of ~IC_{50} concentrations of tropisetron, 6-methoxyharmalan, and harmane on currents activated by EC_{20} (40 μM) glycine in α3-WT GlyRs before and after a 15 min forskolin treatment and a 15 min wash. (B) Averaged data for the experiments shown in (A) (all n = 7). The percentage inhibition produced by the drugs under control conditions was expressed as 100%. The fractional increase in inhibition after phosphorylation is indicated by a corresponding reduction in the percentage current. *p < 0.05, **p < 0.01 relative to control using paired t test.

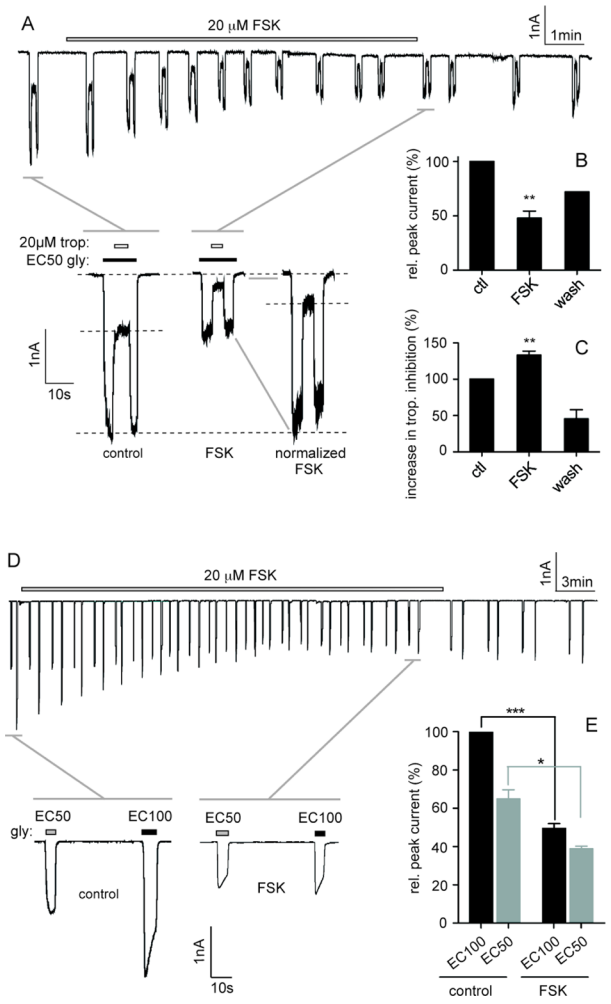

Figure 6. Effects of phosphorylation on α3-WT GlyRs stably expressed in HEK293 cells. (A) Upper panel shows a continuous recording with downward current deflections representing successive activations by EC_{50} (180 μM) glycine, upon each of which is superimposed an ~IC_{50} (20 μM) concentration of tropisetron. The experimental protocol is more readily observed in the two expanded traces below where the glycine and tropisetron applications are indicated by filled and unfilled bars, respectively. The center trace (labeled FSK) has been reproduced (right) normalized to the control trace (left) to emphasize the enhanced inhibition by tropisetron following forskolin exposure. (B) Mean forskolin-induced reduction in current magnitude relative to control averaged from 6 cells for the experiment shown in (A). Partial reversal of the current inhibition by a 15 min wash is also shown. Note that 10 cells were employed in this experiment and 4 cells that elicited no detectable response to forskolin were excluded from analysis. A detectable response was defined as a >10% change in current over a 10 min forskolin application period. (C) Mean forskolin-induced increase in tropisetron-mediated inhibition expressed as a percentage of the control inhibition for the experiment shown in (A). All results were averaged from the same 6 cells as analyzed in (B). (D) Upper panel shows a continuous recording of current activations induced by alternating applications of EC_{50} (150 μM) and EC_{100} (1 mM) glycine. Two sections of this recording are shown expanded below to illustrate the change in magnitudes of the currents following forskolin exposure. (E) Mean forskolin-induced changes in EC_{50} and EC_{100} glycine current magnitudes relative to control. A total of 7 cells was investigated here with 3 eliciting no detectable response to forskolin. Thus, the results represent the average of 4 cells. *p < 0.05, **p < 0.01, ***p < 0.001 relative to control using paired t test.

significantly greater extent than it inhibited EC_{50} currents (Figure 6E), it is evident that glycine sensitivity is actually enhanced by phosphorylation. This allows us to conclude that phosphorylation directly alters tropisetron potency in α3-WT GlyRs.

The main insight of this study is that PKA-dependent phosphorylation of α3 GlyRs produces a conformational change that propagates to the glycine-binding site. Three main lines of evidence support our conclusion that phosphorylation has indeed taken place. First, forskolin is well-known to stimulate cAMP accumulation and thus activate PKA in HEK293 cells. Second, the effect of forskolin on ΔF magnitude in the α3-R19′C GlyR was similar to that of the phosphorylation-mimicking mutation, S346E (Figure 3A, C). Third, forskolin had no effect on ΔF responses in phosphorylation-deficient α3-R19′C-S346G GlyRs or on α1-

dx.doi.org/10.1021/cn400097j | ACS Chem. Neurosci. 2013, 4, 1361−1370

R19′C GlyRs that do not contain an endogenous PKA phosphorylation site.

The present study demonstrates two separable effects of phosphorylation on α3 GlyRs. The first effect, observed only in HEK293 cell-expressed receptors, is the reduced current magnitude. The fact that we observed no effect of phosphorylation on α3 GlyR current magnitudes in *Xenopus* oocytes was fortuitous because it allowed us to eliminate receptor internalization or changes in GlyR open probability as possible explanations for our VCF results. Thus, it permitted us to unequivocally conclude that phosphorylation of S346 exerts a global conformational change that propagates to the α3 GlyR glycine-binding site.

The second effect of phosphorylation, observed in both the HEK293 cell and *Xenopus* oocyte expression systems, is the change in structure at the glycine-binding site. The main lines of evidence in support of this are (1) a phosphorylation-mediated microenvironmental change at a fluorophore attached to loop C of the glycine-binding site and (2) a phosphorylation-mediated enhancement of the inhibitory potency of tropisetron. The magnitude of this potency increase was remarkably similar in the oocyte and HEK293 cell expression systems. Phosphorylation also enhanced receptor sensitivity to glycine in HEK293 cells (Figure 6E), possibly via a similar mechanism.

We speculate that the differential effect of phosphorylation in the two expression systems may be due to differences in the expression levels of one or more intracellular signaling molecules. We propose that S346 phosphorylation, in addition to directly altering glycine-binding site structure, either exposes or occludes a binding site for an expression system-specific intracellular signaling molecule. The subsequent alteration in binding of this molecule to the α3 GlyR thus results in a glycine current magnitude change in HEK293 cells only. The identification of this putative signaling molecule may reveal new therapeutic targets for chronic pain.

It has previously been shown that phosphorylation by PKA or PKC results in the internalization of both recombinant α1 and native neuronal GlyRs.[27,28] We cannot rule internalization out as a possible explanation for the PKA-dependent inhibition of α3 GlyRs we describe in HEK293 cells. We also note that S337, S349, and S380 in the M3-M4 domain of the rat α3L GlyR are also strong phosphorylation consensus sites (Figure S1). Although it is possible they may also contribute to the effects of PKA-dependent phosphorylation, they were not investigated here given that ablation of the S346 phosphorylation site completely eliminated the effects of phosphorylation on α3 GlyR current magnitude.[3]

There is abundant evidence for phosphorylation-induced conformational changes in pLGICs. For example, phosphorylation is known to modify receptor functional properties such as desensitization rate, open probability and surface expression efficiency in 5-HT_3Rs,[29] nAChRs,[26] $GABA_A$Rs,[22−25] and GlyRs.[30,31] However, we are not aware of any evidence for phosphorylation-mediated conformational changes in the M2-M3 loop or neurotransmitter-binding sites of any pLGIC. Considering the importance of the M2-M3 loop and neurotransmitter-binding sites for agonist binding, receptor gating,[12] and desensitization,[32] our findings suggest that these loci could be important sites for investigating the molecular mechanisms by which phosphorylation affects pLGIC structure and function.

Our results may also have clinical significance. For example, as detailed in the Introduction, PGE_2 inhibits α3 GlyRs in spinal nociceptive neurons by phosphorylating S346,[3] thus providing a paradigm for explaining chronic inflammatory pain sensitization.[5,6] Selective enhancement of α3 GlyRs should therefore produce analgesia, and recent evidence indicates that potentiators specific for α3 GlyRs are indeed analgesic in animal models of chronic inflammatory and neuropathic pain.[7] Our finding that the α3 GlyR glycine-binding site is forced into a unique configuration in chronic pain implies that it should be possible to design drugs to selectively potentiate phosphorylated α3 GlyRs, potentially providing a more precisely targeted analgesic therapy. Furthermore, serotonin-1A receptor activation dephosphorylates S346 in α3 GlyRs in brainstem respiratory neurons, thereby increasing glycinergic synaptic current magnitude and counteracting opioid-induced breathing depression.[33] This implies that drugs that selectively potentiate phosphorylated α3 GlyRs may also be efficacious as treatments for opioid-induced breathing disorders.

In conclusion, we have demonstrated that structural changes in the M3-M4 domain can impact on the conformation of the extracellular domains of a pLGIC receptor. In particular, we have shown that phosphorylation of S346 exerts a global conformational change that propagates to the α3 GlyR glycine-binding site. This finding is important for two reasons. First, it provides the first direct evidence for phosphorylation producing extracellular conformational changes in any pLGIC, and thus provides a new locus for investigating how phosphorylation modulates the structure and function of these receptors. Second, it shows that chronic inflammatory pain is accompanied by a unique conformational change in the α3 GlyR glycine-binding site, which raises the possibility of developing analgesic drugs to specifically target disease-affected receptors.

METHODS

Chemicals. MTSR and TAMRA were obtained from Toronto Research Chemicals. Glycine, β-alanine, taurine, ivermectin, picrotoxin, strychnine, forskolin, tropisetron, harmane, and 6-methoxyharmalan were all obtained from Sigma. Glycine, β-alanine, taurine, and strychnine were dissolved in water. All other drugs were prepared as 20−100 mM stocks in dimethyl sulfoxide and kept frozen at −20 °C. From these stocks, solutions for experiments were prepared on the day of recording.

Molecular Biology. Plasmid DNAs for the human α1 and rat α3L GlyR subunits were kindly provided by Prof. Peter Schofield (Neuroscience Research Australia) and Prof. Robert Harvey (University College, London), respectively. For *Xenopus* oocyte recordings, the subunit DNAs were subcloned into pGEMHE, a plasmid vector optimized for oocyte expression. The α1 and α3L constructs both incorporated the C41A mutation that eliminated the sole uncross-linked extracellular sulfhydryl group. Site directed mutagenesis was performed using the QuikChange mutagenesis kit (Stratagene). Successful incorporation of the mutations was confirmed through automated sequencing of the entire cDNA coding region. Chimeras were constructed using a multiple-template-based sequential PCR protocol as recently described.[34] The join sites between the α1 and α3 sequences used to create chimeras Chi1−Chi6 were located between the following pairs of residues: α1 Y223/L224 and α3 Y223/L224 for the N terminal end of M1, and α1 R392/I393 and α3 R400/A401 for the C terminal end of the M3-M4 loop (Figure S1). ChiA involved inserting the α3 GlyR residues K322−R400, inclusive, in place of α1 GlyR residues R322−R392, inclusive. ChiB incorporated the reverse domain substitution.

Ten micrograms of each cDNA was linearized by NheI or PstI and then purified by using a PCR-purification kit (Qiagen). The capped RNAs were transcribed from cDNA using the Ambion T7 mMessage mMachine kit, purified by using the RNAMinikit (Qiagen) eluted with

DNA/RNAase free water and diluted to 200 ng/μL for oocyte injection.

Oocyte Preparation, Injection, and Labeling. Female *Xenopus laevis* frogs (*Xenopus* Express) were anesthetized with 5 mM MS-222 (Sigma Aldrich), and stage VI oocytes were removed from ovaries and washed thoroughly in OR-2 (82.5 mM NaCl, 2 mM KCl, 1 mM $MgCl_2$, 5 mM HEPES, pH 7.4). The oocytes were then incubated in collagenase (Sigma Aldrich) in OR-2 for 2 h at room temperature, rinsed and stored in OR-2 at 18 °C.

All oocytes were injected with 10 ng of mRNA into the cytosol. To achieve the high levels of expression required for the detection of the fluorescent signal over the background (due to oocyte autofluorescence and nonspecific binding of the dye), the oocytes were incubated at 18 °C for 3−10 days after injection. The incubation solution contained 96 mM NaCl, 2 mM KCl, 1 mM $MgCl_2$, 1.8 mM $CaCl_2$, 5 mM HEPES, 0.6 mM theophylline, 2.5 mM pyruvic acid, 50 μg/mL gentamycin (Cambrex Corporation), and 5% horse serum (Hycell), at pH 7.4.

On the day of recording, the oocytes were transferred into ND96 (96 mM NaCl, 2 mM KCl, 1 mM $MgCl_2$, 1.8 mM $CaCl_2$, 5 mM HEPES, pH 7.4) and stored on ice. To label with either MTSR or MTS-TAMRA, oocytes were transferred into the labeling solution containing 10 μM of either compound in ND96 for 25 s. The oocytes were then washed and stored in ND96 for up to 6 h before recording. All labeling steps were performed on ice.

VCF. We employed an inverted microscope (Eclipse TE300, Nikon Instruments) equipped with a high-Q tetramethylrhodamine isothiocyanate filter set (Chroma Technology), a Plan Fluor 40× objective (Nikon Instruments) and an H7360-03 photomultiplier detection system (Hamamatsu Photonics) attached to the side port of the microscope. An excitation filter wheel including a shutter and an emission filter wheel were controlled through a Lambda 10-2 unit (Sutter Instruments). A Lambda LS 175 W xenon arc lamp served as a light source and was coupled to the microscope via a liquid light guide (Sutter Instruments). The design of the custom-made recording chamber has been described previously.[35] An automated perfusion system operated by a ValveBank-8 valve controller (AutoMate Scientific) was used for perfusion of the recording chamber. Electrodes for two-electrode voltage clamp recordings were filled with 3 M KCl and moved by automated ROE-200 micromanipulators coupled to an MPC-200 controller (Sutter Instruments). Cells were voltage-clamped at −40 mV and currents were recorded using a Gene Clamp 500B amplifier (Molecular Devices). Current and fluorescence traces were acquired at 200 Hz via a Digidata 1322A interface and Clampex 9.2 software.

HEK293 Cell Culture. We employed HEK293 cell lines that stably expressed either α1 or α3L GlyRs. Generation of these cell lines has previously been described.[36] Cells were cultured on glass coverslips in Dulbecco's modified Eagle's medium supplemented with G-418 (1 mg/mL), penicillin (100 U/ml), streptomycin (100 mg/mL). and 10% Serum Supreme and maintained at 37 °C in a 5% CO_2 incubator.

Patch Clamp Electrophysiology. Cells were viewed using an inverted microscope, and currents were recorded by whole-cell patch-clamp recording. Cells were perfused by an extracellular solution containing (in mM): 140 NaCl, 5 KCl, 2 $CaCl_2$, 1 $MgCl_2$, 10 HEPES/NaOH, and 10 glucose (pH 7.4 adjusted with NaOH). Patch pipettes were fabricated from borosilicate hematocrit tubing (Hirschmann Laborgerate) and heat polished. Pipettes had a tip resistance of 1−2 MΩ when filled with the intracellular solution consisting of (mM): 145 CsCl, 2 $CaCl_2$, 2 $MgCl_2$, 10 HEPES, and 10 EGTA (pH 7.4 adjusted with CsOH). After establishment of the whole-cell recording configuration, cells were voltage clamped at −40 mV and membrane currents were recorded using an Axopatch 200C and pClamp 10 software (Molecular Devices). Currents were filtered at 500 Hz and digitized at 2 kHz.

Solutions were applied to cells via gravity forced perfusion and parallel microtubules and manual control of this system was achieved via a micromanipulator with a solution exchange time of <250 ms. Experiments were conducted at room temperature (19−22 °C).

Data Analysis. EC_{50} and n_H values for ligand-induced activation of ΔI and ΔF signals were obtained using the empirical Hill equation, fitted with a nonlinear least-squares algorithm (SigmaPlot 12.0, Systat Software). All results are expressed as mean ± standard error of the mean (SEM) of three or more independent experiments. All dose−responses relations were fitted using a nonlinear least-squares algorithm (Sigmaplot 12.0). Unless otherwise indicated, statistical significance was determined by Student's t test with $p < 0.05$ representing significance.

■ ASSOCIATED CONTENT

Supporting Information

Additional tables and figures as described in the text. This material is available free of charge via the Internet at http://pubs.acs.org.

■ AUTHOR INFORMATION

Corresponding Author

*Telephone: (+617) 33466375. Fax: (+617) 33466301. E-mail: j.lynch@uq.edu.au.

Present Address

[§]Q.S.: Brain and Mind Research Institute, University of Sydney, Sydney, NSW 2050, Australia.

Author Contributions

Participated in research design: H.L., Q.S., and J.W.L. Provided expertise in generating molecular constructs: Q.S. Conducted experiments and performed data analysis: H.L., Q.W., and S.T. Wrote manuscript: L.H., S.T., and J.W.L.

Funding

Funding for this research was received from the Australian Research Council and the National Health and Medical Research Council of Australia.

Notes

The authors declare no competing financial interest.

■ ABBREVIATIONS

5-HT_3R, 5-hydroxytryptamine type-3 receptor; ΔF, change in fluorescence; ΔF_{max}, maximum change in fluorescence; ΔI, change in current; ΔI_{max}, maximum change in current; $GABA_A$R, gamma-aminobutyric acid type-A receptor; GluClR, glutamate-gated chloride channel receptor; GlyR, glycine receptor; MTSR, rhodamine methanethiosulfonate; MTS-TAMRA, 2-((5(6)-tetramethylrhodamine)carboxylamino)ethyl methanethiosulfonate; nAChR, nicotinic acetylcholine receptor; PGE_2, prostaglandin E_2; PKA, protein kinase A; pLGIC, pentameric ligand-gated ion channel; TM, transmembrane; VCF, voltage-clamp fluorometry

■ REFERENCES

(1) Webb, T. I., and Lynch, J. W. (2007) Molecular pharmacology of the glycine receptor chloride channel. *Curr. Pharm. Des. 13*, 2350−2367.

(2) Rajendra, S., Vandenberg, R. J., Pierce, K. D., Cunningham, A. M., French, P. W., Barry, P. H., and Schofield, P. R. (1995) The unique extracellular disulfide loop of the glycine receptor is a principal ligand binding element. *EMBO J. 14*, 2987−2998.

(3) Harvey, R. J., Depner, U. B., Wassle, H., Ahmadi, S., Heindl, C., Reinold, H., Smart, T. G., Harvey, K., Schutz, B., Abo-Salem, O. M., Zimmer, A., Poisbeau, P., Welzl, H., Wolfer, D. P., Betz, H., Zeilhofer, H. U., and Muller, U. (2004) GlyR alpha3: an essential target for spinal PGE2-mediated inflammatory pain sensitization. *Science 304*, 884−887.

(4) Ahmadi, S., Lippross, S., Neuhuber, W. L., and Zeilhofer, H. U. (2002) PGE(2) selectively blocks inhibitory glycinergic neuro-

transmission onto rat superficial dorsal horn neurons. *Nat. Neurosci. 5*, 34−40.
(5) Lynch, J. W., and Callister, R. J. (2006) Glycine receptors: a new therapeutic target in pain pathways. *Curr. Opin. Invest. Drugs 7*, 48−53.
(6) Zeilhofer, H. U. (2005) The glycinergic control of spinal pain processing. *Cell. Mol. Life Sci. 62*, 2027−2035.
(7) Xiong, W., Cui, T., Cheng, K., Yang, F., Chen, S. R., Willenbring, D., Guan, Y., Pan, H. L., Ren, K., Xu, Y., and Zhang, L. (2012) Cannabinoids suppress inflammatory and neuropathic pain by targeting alpha3 glycine receptors. *J. Exp. Med. 209*, 1121−1134.
(8) Lynch, J. W., Han, N. L., Haddrill, J., Pierce, K. D., and Schofield, P. R. (2001) The surface accessibility of the glycine receptor M2-M3 loop is increased in the channel open state. *J. Neurosci. 21*, 2589−2599.
(9) Pless, S. A., Dibas, M. I., Lester, H. A., and Lynch, J. W. (2007) Conformational variability of the glycine receptor M2 domain in response to activation by different agonists. *J. Biol. Chem. 282*, 36057−36067.
(10) Han, N. L., Clements, J. D., and Lynch, J. W. (2004) Comparison of taurine- and glycine-induced conformational changes in the M2-M3 domain of the glycine receptor. *J. Biol. Chem. 279*, 19559−19565.
(11) Lynch, J. W., Rajendra, S., Pierce, K. D., Handford, C. A., Barry, P. H., and Schofield, P. R. (1997) Identification of intracellular and extracellular domains mediating signal transduction in the inhibitory glycine receptor chloride channel. *EMBO J. 16*, 110−120.
(12) Miller, P. S., and Smart, T. G. (2010) Binding, activation and modulation of Cys-loop receptors. *Trends Pharmacol. Sci. 31*, 161−174.
(13) Shan, Q., Haddrill, J. L., and Lynch, J. W. (2001) Ivermectin, an unconventional agonist of the glycine receptor chloride channel. *J. Biol. Chem. 276*, 12556−12564.
(14) Lynagh, T., and Lynch, J. W. (2010) An improved ivermectin-activated chloride channel receptor for inhibiting electrical activity in defined neuronal populations. *J. Biol. Chem. 285*, 14890−14897.
(15) Unwin, N. (2005) Refined structure of the nicotinic acetylcholine receptor at 4A resolution. *J. Mol. Biol. 346*, 967−989.
(16) Celie, P. H., Kasheverov, I. E., Mordvintsev, D. Y., Hogg, R. C., van Nierop, P., van Elk, R., van Rossum-Fikkert, S. E., Zhmak, M. N., Bertrand, D., Tsetlin, V., Sixma, T. K., and Smit, A. B. (2005) Crystal structure of nicotinic acetylcholine receptor homolog AChBP in complex with an alpha-conotoxin PnIA variant. *Nat. Struct. Mol. Biol. 12*, 582−588.
(17) Bourne, Y., Talley, T. T., Hansen, S. B., Taylor, P., and Marchot, P. (2005) Crystal structure of a Cbtx-AChBP complex reveals essential interactions between snake alpha-neurotoxins and nicotinic receptors. *EMBO J. 24*, 1512−1522.
(18) Pless, S. A., and Lynch, J. W. (2009) Ligand-specific conformational changes in the alpha 1 glycine receptor ligand-binding domain. *J. Biol. Chem. 284*, 15847−15856.
(19) Chen, X., Cromer, B. A., and Lynch, J. W. (2009) Molecular determinants of beta-carboline inhibition of the glycine receptor. *J. Neurochem. 110*, 1685−1694.
(20) Maksay, G., Laube, B., Schemm, R., Grudzinska, J., Drwal, M., and Betz, H. (2009) Different binding modes of tropeines mediating inhibition and potentiation of alpha1 glycine receptors. *J. Neurochem. 109*, 1725−1732.
(21) Yang, Z., Ney, A., Cromer, B. A., Ng, H. L., Parker, M. W., and Lynch, J. W. (2007) Tropisetron modulation of the glycine receptor: femtomolar potentiation and a molecular determinant of inhibition. *J. Neurochem. 100*, 758−769.
(22) Abramian, A. M., Comenencia-Ortiz, E., Vithlani, M., Tretter, E. V., Sieghart, W., Davies, P. A., and Moss, S. J. (2010) Protein kinase C phosphorylation regulates membrane insertion of GABAA receptor subtypes that mediate tonic inhibition. *J. Biol. Chem. 285*, 41795−41805.
(23) Houston, C. M., and Smart, T. G. (2006) CaMK-II modulation of GABA(A) receptors expressed in HEK293, NG108−15 and rat cerebellar granule neurons. *Eur. J. Neurosci. 24*, 2504−2514.
(24) McDonald, B. J., Amato, A., Connolly, C. N., Benke, D., Moss, S. J., and Smart, T. G. (1998) Adjacent phosphorylation sites on GABAA receptor beta subunits determine regulation by cAMP-dependent protein kinase. *Nat. Neurosci. 1*, 23−28.
(25) Saliba, R. S., Kretschmannova, K., and Moss, S. J. (2012) Activity-dependent phosphorylation of GABAA receptors regulates receptor insertion and tonic current. *EMBO J. 31*, 2937−2951.
(26) Swope, S. L., Moss, S. J., Raymond, L. A., and Huganir, R. L. (1999) Regulation of ligand-gated ion channels by protein phosphorylation. *Adv. Second Messenger Phosphoprotein Res. 33*, 49−78.
(27) Huang, R., He, S., Chen, Z., Dillon, G. H., and Leidenheimer, N. J. (2007) Mechanisms of homomeric alpha1 glycine receptor endocytosis. *Biochemistry 46*, 11484−11493.
(28) Velazquez-Flores, M. A., and Salceda, R. (2011) Glycine receptor internalization by protein kinases activation. *Synapse 65*, 1231−1238.
(29) Yakel, J. L., Shao, X. M., and Jackson, M. B. (1991) Activation and desensitization of the 5-HT3 receptor in a rat glioma x mouse neuroblastoma hybrid cell. *J. Physiol. 436*, 293−308.
(30) Legendre, P. (2001) The glycinergic inhibitory synapse. *Cell. Mol. Life Sci. 58*, 760−793.
(31) Lynch, J. W. (2004) Molecular structure and function of the glycine receptor chloride channel. *Physiol. Rev. 84*, 1051−1095.
(32) Wang, Q., and Lynch, J. W. (2011) Activation and desensitization induce distinct conformational changes at the extracellular-transmembrane domain interface of the glycine receptor. *J. Biol. Chem. 286*, 38814−38824.
(33) Manzke, T., Niebert, M., Koch, U. R., Caley, A., Vogelgesang, S., Hulsmann, S., Ponimaskin, E., Muller, U., Smart, T. G., Harvey, R. J., and Richter, D. W. (2010) Serotonin receptor 1A-modulated phosphorylation of glycine receptor alpha3 controls breathing in mice. *J. Clin. Invest. 120*, 4118−4128.
(34) Shan, Q., and Lynch, J. W. (2010) Chimera construction using multiple-template-based sequential PCRs. *J. Neurosci. Methods 193*, 86−89.
(35) Dahan, D. S., Dibas, M. I., Petersson, E. J., Auyeung, V. C., Chanda, B., Bezanilla, F., Dougherty, D. A., and Lester, H. A. (2004) A fluorophore attached to nicotinic acetylcholine receptor beta M2 detects productive binding of agonist to the alpha delta site. *Proc. Natl Acad. Sci. U.S.A. 101*, 10195−10200.
(36) Balansa, W., Islam, R., Fontaine, F., Piggott, A. M., Zhang, H., Webb, T. I., Gilbert, D. F., Lynch, J. W., and Capon, R. J. (2010) Ircinialactams: subunit-selective glycine receptor modulators from Australian sponges of the family Irciniidae. *Bioorg. Med. Chem. 18*, 2912−2919.
(37) Han, L., Talwar, S., and Lynch, J. W. (2013) The relative orientation of the TM3 and TM4 domains varies between alpha1 and alpha3 glycine receptors. *ACS Chem. Neurosci. 4*, 248−254.